

pubs.acs.org/acsapm Forum Article

Comparative Study of Selenophene- and Thiophene-Containing n-Type Semiconducting Polymers for High Performance All-Polymer Solar Cells

Xiaomei Ding, Duyen K. Tran, Daiki Kuzuhara, Tomoyuki Koganezawa, and Samson A. Jenekhe*



Cite This: https://dx.doi.org/10.1021/acsapm.0c00772



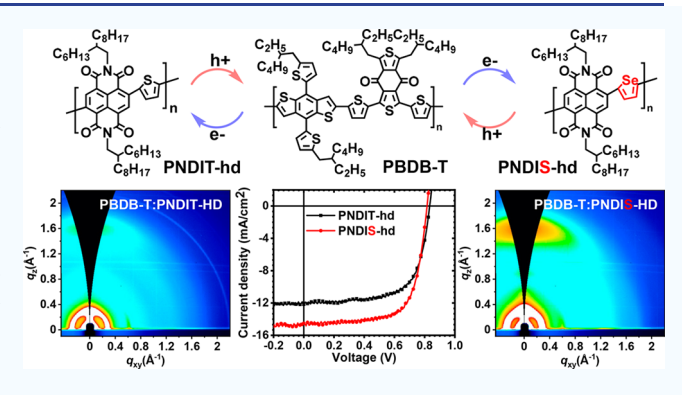
ACCESS

Metrics & More

Article Recommendations

s Supporting Information

ABSTRACT: Effects of the donor moiety substitution on the intrinsic and photovoltaic blend properties of n-type semiconducting naphthalene diimide-arylene copolymers with donor—acceptor structure were investigated. The alternating naphthalene diimide-thiophene copolymer, PNDIT-hd, and naphthalene diimide-selenophene copolymer, PNDIS-hd, were found to have identical electrochemically derived electronic structures and similar bulk electron mobility; however, PNDIS-hd has an optical bandgap of 1.70 eV, which is 0.07 eV narrower relative to that of PNDIT-hd. All-polymer solar cells incorporating the donor polymer, PBDB-T, and PNDIS-hd were found to combine a high power conversion efficiency of 8.4% with high external quantum efficiency (86%) and a high fill factor of 0.71,



which are significantly enhanced compared to the corresponding PBDB-T:PNDIT-hd devices with 6.7% power conversion efficiency and 73% external quantum efficiency. The improved photovoltaic properties of the selenophene-containing acceptor copolymer relative to the thiophene counterpart originate from enhanced light harvesting, more favorable molecular packing in blends, and reduced charge recombination losses in devices. These findings demonstrate that selenophene substitution for thiophene in donor—acceptor copolymers is an effective strategy that enhances the intrinsic polymer properties as well as the performance of all-polymer solar cells incorporating them.

KEYWORDS: all-polymer solar cells, n-type semiconducting polymer, naphthalenediimide-selenophene copolymer, naphthalenediimide-thiophene copolymer, blend morphology, donor—acceptor copolymer, electron transport

■ INTRODUCTION

All-polymer solar cells (all-PSCs)^{1–20} are typically composed of a binary blend of two different conjugated polymers, one that functions as a p-type semiconductor, and the other that functions as an n-type semiconductor. As a special class of organic photovoltaics, all-PSCs have many unique advantages, including their excellent mechanical properties; their rugged thermo-mechanical stability; the great potential for their integration into buildings, textiles, and other structures; scalable and cost-effective manufacturing of the devices; and the facile tunability of the properties of polymeric materials.^{1–5,21,22} Although progress in increasing the power conversion efficiency (PCE) of all-PSCs was relatively slow for a long time compared to polymer/fullerene devices,²³ the last 7 years has seen rapid advances largely due to the emergence of new generations of n-type semiconducting polymers.^{1–5} Indeed, the efficiency of all-PSCs has climbed from below 2%^{4,6} in 2012 to 8%^{9,24} in 2015 and to over 10–14% recently.^{10,14,17–20,25}

The new generations of both p-type and n-type semiconducting polymers that have enabled advances in the performance of polymer solar cells, including all-PSCs, in the last two decades have emerged from a powerful macromolecular design strategy, the so-called "donor—acceptor (D—A) architecture", ²⁶ whereby the conjugated copolymer repeat unit is composed of alternating electron-donating (D) and electron-accepting (A) moieties of varying complexities and permutations. ^{27–29} The modular nature of such D–A conjugated copolymers has enabled the facile tuning of the electronic band structure, light-harvesting properties, and charge transport properties of the materials. A general feature of all D–A copolymers is that they exhibit an intramolecular charge transfer (ICT) band in their optical absorption spectra, whose strength and spectral range depend on the strength of

Special Issue: High Efficiency Polymers for Solar Cell

Applications

Received: July 15, 2020 Accepted: September 3, 2020



the ICT interaction. ^{26,27} The relative strengths of the electron-deficient moiety A and electron-donating moiety D incorporated into the D–A conjugated copolymer determine the electronic band structure, including the electron affinity and ionization energy or HOMO/LUMO energy levels, and thus whether the material will be primarily a p-type or n-type semiconductor or even an ambipolar semiconductor. ^{30,31} Numerous p-type semiconducting polymers with D–A architectures that have high bulk hole mobility and suitable HOMO energy level (<–5.0 eV) have been initially developed for applications in polymer/fullerene solar cells. ²³ Although lagging behind their p-type counterparts, many n-type semiconducting polymers with D–A architectures that have high bulk electron mobility and suitable LUMO energy level (<–3.4 eV) have similarly been developed, and these have enabled advances in all-PSCs. ^{1–20,32,33}

Arylene diimides,³⁴ including naphthalene diimide (NDI),^{7-9,35} perylene diimide (PDI),⁸ tetraazabenzo-difluoranthene diimide (BFI),³⁶⁻³⁸ naphtho-dithiophenediimide (NDTI),³⁹⁻⁴¹ and bithiophene diimide (BTI), 42-44 are the most widely investigated electron-deficient building blocks "A" in the design of n-type semiconducting copolymers with D-A architectures for applications in all-PSCs. 1-20 Currently, NDI-based D-A copolymers have been the most widely studied and successful class of n-type semiconducting (or acceptor) polymers for all-PSCs due to their combination of large electron affinity, high electron mobility, and excellent self-assembly and semicrystalline properties.^{34,45} Although early studies of NDI-based D-A copolymers focused on understanding the effects of the choice of various donor moieties on the HOMO/LUMO energy levels, the tendency toward unipolar or ambipolar charge transport, and carrier mobility, 30,46,47 recent applications in all-PSCs have largely focused on bithiophene-NDI, biselenophene-NDI, and related random copolymers, which have enabled solar cell efficiencies above 9–10%. 7,16,25,48 Here, our primary goal is to explore the effects of the donor moiety substitution on the intrinsic and photovoltaic blend properties of n-type semiconducting polymers with the simplest possible D-A macromolecular structure based on the NDI acceptor moiety, i.e. (-D-NDI-), where the donor moiety "D" is a simple unicyclic ring such as thiophene or selenophene. For example, the nature and strength of the ICT interaction, intermolecular interactions, the molecular packing and electronic properties of (-D-NDI-)-type polymers can be expected to be very different compared to those with (-D-D-NDI-) structure.^{7,46} Hence, relative to the more widely studied but more complex (-D-D-NDI-) architectures such as bithiophene-NDI and biselenophene-NDI, 7,46 we expect a comparative study of (-D-NDI-) type structures to provide new insights for the design and application of semiconducting polymers with D-A architectures.

In this paper, we report a comparative study of alternating naphthalene diimide-thiophene copolymer (PNDIT-hd) and naphthalene diimide-selenophene copolymer (PNDIS-hd) as model (-D-NDI-) type D-A copolymer acceptors, whose molecular structures are shown in Figure 1, in all-PSCs. The backbone substitution of selenophene for thiophene in going from PNDIT-hd to PNDIS-hd was found to have minimal impact on the HOMO/LUMO energy levels of the n-type semiconducting copolymers. However, the thin-film optical absorption spectrum of PNDIS-hd was slightly red-shifted, resulting in a 0.07 eV decrease of optical bandgap relative to

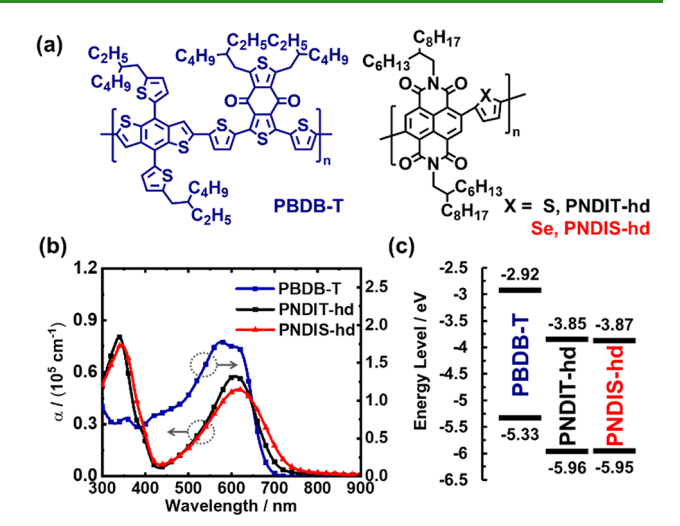


Figure 1. (a) Molecular structures, (b) thin-film optical absorption spectra, and (c) HOMO/LUMO energy levels of acceptor polymers PNDIT-hd and PNDIS-hd and donor polymer PBDB-T.

PNDIT-hd. Binary blends of PNDIT-hd and PNDIS-hd respectively with the wide-bandgap donor polymer PBDB-T^{49,50} (Figure 1) produced all-PSCs in which the selenophene-containing acceptor polymer significantly improved photo-current and overall photovoltaic power conversion efficiency. PNDIT-hd:PBDB-T-based all-PSCs could thus achieve a PCE of 6.7% ($J_{\rm sc}=12.18~{\rm mA/cm^2}$, FF = 0.66), whereas the corresponding PNDIS-hd:PBDB-T devices showed a higher PCE of 8.4% ($J_{\rm sc}=14.50~{\rm mA/cm^2}$, FF = 0.71). The observed enhanced photovoltaic properties of the selenophene-containing polymer PNDIS-hd are largely accounted for by the improved light harvesting and formation of optimal blend morphology compared to its thiophene counterpart, PNDIT-hd

■ EXPERIMENTAL METHODS

Materials and Characterization. The donor polymer PBDB-T was purchased from Brilliant Matters Inc. (Quebec, Canada): $M_n = 60$ kDa, D = 1.9, metallic impurities content <0.01%. The acceptor polymers, PNDIT-hd and PNDIS-hd, were synthesized according to our previous report.^{6,9} The molecular structures of PNDIT-hd and PNDIS-hd were confirmed by ¹H NMR spectra, which are provided in the Supporting Information. The molecular weight of the acceptor polymers was characterized by gel-permeation chromatography (GPC) against polystyrene standards and eluting with chloroform at room temperature: PNDIT-hd ($M_{\rm n}$ = 10.0 kDa, $M_{\rm w}$ = 21.0 kDa, D = 2.10), PNDIS-hd ($M_n = 22.1 \text{ kDa}$, $M_w = 64.9 \text{ kDa}$, D = 2.94). Thermogravimetric analysis (TGA) of the polymers was conducted on a TA Instruments model Q50 TGA at a heating rate of 10 °C/min under a flow of N₂ with scans from room temperature to 800 °C. Differential scanning calorimetry (DSC) analysis was performed on a TA Instruments model Q100 DSC under N2 by scanning from 20 to 400 °C at a heating rate of 20 °C/min. Optical absorption spectra were obtained from a PerkinElmer Lambda 900 UV-vis/near-IR spectrophotometer.

The HOMO/LUMO energy levels of the polymers were determined from cyclic voltammetry (CV) experiments performed on an EG&G Princeton Applied Research potentiostat/galvanostat (model 273A). A three-electrode cell was used, using platinum (Pt) wires as both counter and working electrodes. Silver/silver ion (Ag in 0.01 M AgNO $_3$ solution) was used as the reference electrode. The working electrode was a Pt wire coated with a polymer thin film dip coated from each polymer solution in chlorobenzene (PNDIT-hd, PNDIS-hd, and PBDB-T). All the CV measurements were carried out

in 0.1 M tetrabutylammonium hexafluorophosphate (Bu₄NPF₆) solution in acetonitrile at a scan rate of 50 mV/s. The reduction and oxidation potentials were referenced to the ferrocene-ferrocenium (Fc/Fc⁺) couple by using ferrocene as an internal standard; to derive the HOMO/LUMO energy levels from the redox potentials, HOMO energy level of ferrocene is taken to be at -4.8 eV relative to the vacuum level. The Fc/Fc⁺ couple was found at 0.09 V in our experiments. Thus, the LUMO and HOMO energy levels of the semiconducting polymers investigated were determined by using following relationships: $E_{\rm LUMO} = -(E_{\rm red}^{\rm onset} + 4.71)$ eV and $E_{\rm HOMO} = -(E_{\rm ox}^{\rm onset} + 4.71)$ eV, respectively.

Solar Cell Fabrication and Testing. The inverted all-PSC device structure fabricated and evaluated was: ITO/ZnO/PEI/blend active layer/MoO₃(0.5 nm)/Ag(100 nm), where PEI or polyethylenimine is a cathode buffer layer. The ITO glass substrates were sequentially sonicated in acetone, deionized (DI) water, and isopropanol for 20 min each and then plasma cleaned for 10 min. The ZnO layer (~30 nm) was spin-coated from the precursor solution (0.5 g of zinc acetate dihydrate, 0.14 g of ethanolamine and 5 mL of 2-methoxyethanol) and baked at 250 °C for 30 min in open air. A solution of PEI ($M_{\rm w}=25{\rm k}$, Aldrich 408727) in 2-methoxyethanol (0.05 wt %) was then spin-coated onto the ZnO layer and dried at 120 °C for additional 10 min. The resulting substrates were then stored in an argon-filled glovebox for deposition of active layers.

The active layer blend solution was prepared by mixing a chlorobenzene solution of the donor polymer PBDB-T (10 mg/ mL) respectively with a chlorobenzene solution of PNDIT-hd (25 mg/mL) or PNDIS-hd (20 mg/mL); various solution volumes of the component polymers were mixed in the right proportions to afford the desired blend film compositions. In cases where a diphenyl ether (DPE) processing additive was used, the chlorobenzene:DPE (v/v %) mixed solvent was achieved by adding the DPE to a prepared blend solution. The blend solutions were stirred overnight with low heating to achieve a homogeneous mixture. Each blend solution was then spin-coated onto the cleaned substrate and annealed on a hot plate for 10 min to afford dried thin films with a thickness of 95 \pm 5 nm. Finally, the MoO₃ layer and Ag electrode were deposited within a thermal evaporator. Defined active area of 0.0314 cm² was achieved for individual devices through a shadow mask. The photovoltaic cells were tested under AM 1.5G solar illumination at 100 mW/cm² in ambient air using a Solar Simulator (model 16S, Solar Light Co., Philadelphia, PA) with a 200 W xenon Lamp Power Supply (Model XPS 200, Solar Light Co., Philadelphia, PA) calibrated by NREL certified Si photodiode (Model 1787-04, Hamamatsu Photonics K.K., Japan) and a HP4155A semiconductor parameter analyzer (Yokogawa Hewlett-Packard, Japan). After the current-voltage (J-V) measurement, the external quantum efficiency (EQE) was measured by using a solar cell quantum efficiency measurement system (Model QEX10, PV Measurements, Inc., Boulder, CO) with a 2 mm² (2 \times 1 mm) size masked incident light source and TF Mini Super measurement apparatus for multiple devices in a single substrate.

SCLC Device Fabrication and Testing. The space charge limited current (SCLC)⁵² devices fabricated and evaluated had the structures: ITO/PEDOT: PSS/blend/MoO₃ (7.5 nm)/Ag (100 nm) (hole-only), where poly(3,4-ethylenedioxythiophene):poly(styrenesulfonate) (PEDOT:PSS) is a hole injection layer, and ITO/ZnO/PEI/blend/LiF(1 nm)/Al(100 nm) (electron-only). The blend active layers in these SCLC devices had the same composition as the corresponding photovoltaic devices. J-V characteristics of the SCLC devices were plotted as $J^{0.5}$ versus V and fitted by using the following formula: $J = 9\varepsilon_0\varepsilon_x\mu V^2/8d^3$, where J is the current density, ε_0 is the permittivity of free space, ε_r is the relative dielectric constant of the transport medium, μ is the carrier mobility, V is the applied voltage, and d is the thickness of blend active layer.

Atomic Force Microscopy (AFM) Imaging. The surfaces of the actual all-polymer solar cell devices were imaged by using the atomic force microscope (Model: Bruker Dimension ICON).

2D GIWAXS Measurements. Grazing incidence X-ray scattering (GIWAXS) experiments were conducted at the Japan Synchrotron Radiation Facility SPring-8 by using the beamline BL46XU. The thin-

film samples investigated were prepared in the same manner as the corresponding photovoltaic devices on ZnO-coated ITO substrates, without the thermal deposition of top MoO₃/Ag electrodes. The X-ray beam was monochromatized by a double-crystal Si(111) monochromator, and the X-ray energy in this experiment was 12.40 keV ($\lambda=0.1$ nm). The angle of incident X-ray to sample surface was 0.12° with a Huber diffractometer. The scattered profile from the film sample was detected using an area detector (PILATUS 300 K) for 5 s at room temperature, and the distance between the sample and detector was 174.4 mm. The crystalline coherence length ($L_{\rm c}$) of samples was determined by using the Scherrer equation: $L_{\rm c}=2\pi K/\Delta q$, where K is a shape factor (typically 0.89) and Δq is the full width at half-maximum (fwhm) of the diffraction peak. Here, the $L_{\rm c}(100)$ was obtained from the fwhm of the (100) diffraction peak in the inplane (q_{xy}) line cut.

RESULTS AND DISCUSSION

Synthesis and Characterization of Acceptor Polymers. The acceptor polymers PNDIT-hd and PNDIS-hd were synthesized by using a Stille copolymerization approach according to the procedures of previous reports.^{6,9} The molecular structures of both polymers were confirmed by ¹H NMR spectra (Figures S1 and S2). The polymers are readily soluble in common organic solvents such as chloroform (CF) and chlorobenzene (CB). The molecular weight of the polymers was determined by GPC eluting with chloroform at room temperature. The number-average molecular weight (M_n) of PNDIT-hd and PNDIS-hd was 10.0 and 22.1 kDa, with dispersity (D) of 2.10 and 2.94, respectively (Table S1). These M_n values of both PNDIT-hd and PNDIS-hd are within the low range of polymer molecular weight (<30 kDa) and therefore are not expected to influence variation in morphology and photovoltaic performance. 53,54 TGA showed that the decomposition temperature (5% weight loss) is 442 °C for PNDIT-hd and 401 °C for PNDIS-hd (Figure S3a), indicating excellent thermal stability of both acceptor polymers. DSC scans showed that PNDIS-hd has broad melting peaks at 315 and 335 °C and a broad recrystallization peak over the range of 320-290 °C in the cooling scan (Figure S3b). In contrast, PNDIT-hd showed melting transition peak in the 260-270 °C range and a relatively sharp recrystallization peak at 246 °C. The significantly higher melt transition temperature of the selenophene-containing PNDIS-hd implies stronger intermolecular interactions due to Se–Se interactions, 45,55 given that both polymers (PNDIS-hd and PNDIThd) are otherwise similar in molecular structure.

The thin-film optical absorption spectra of the acceptor polymers PNDIT-hd and PNDIS-hd are shown in Figure 1b, while those in dilute (10^{-6} M) chlorobenzene solutions are shown in Figure S4. The absorption spectra are similar to those in previous reports, ^{6,56} with both PNDIT-hd and PNDIS-hd showing two characteristic absorption peaks, one centered at 320–350 nm attributed to the π - π * transition and the other at 540–610 nm due to intramolecular charge transfer (ICT). ^{26,27} In both dilute solution and thin film, PNDIS-hd exhibits a broader absorption band than PNDIT-hd, in agreement with previous reports ^{6,56} that showed that selenophene substitution for the thiophene ring can slightly enhance light-harvesting. The bandgap ($E_{\rm g}$) derived from the thin-film optical absorption edge was 1.77 eV for PNDIT-hd and 1.70 eV for PNDIS-hd (Figure 1b and Table S1).

The HOMO/LUMO energy levels of the acceptor polymers were determined from CV experiments (Figure S5), and relevant data are listed in Table S1. The HOMO/LUMO

Table 1. Summary of Photovoltaic Properties of PNDIT-hd:PBDB-T and PNDIS-hd:PBDB-T Blends

blend	DPE (%)	$J_{\rm sc}~({\rm mA/cm^2})$	$V_{\rm oc}$ (V)	FF	$PCE_{max} (PCE_{avg}^{c}) (\%)$	EQE_{max} (%)	Int $J_{\rm sc}$ (mA/cm ²)
PNDIT-hd ^a		11.45	0.83	0.68	$6.52 (6.35 \pm 0.14)$	70.0	11.16
PNDIT-hd ^a	1	12.18	0.83	0.66	$6.74 (6.46 \pm 0.14)$	72.9	11.57
PNDIS-hd ^b		14.29	0.82	0.68	$8.01 \ (7.72 \pm 0.26)$	83.2	13.71
PNDIS-hd ^b	0.5	14.50	0.82	0.71	$8.36 (8.05 \pm 0.19)$	85.7	14.22

^aAnnealed at 155 °C for 10 min. ^bAnnealed at 135 °C for 10 min. ^cAverage of over 10 devices.

values observed, -5.96/-3.85 eV for PNDIT-hd and -5.95/-3.87 eV for PNDIS-hd, are essentially identical, which suggests that selenophene substitution for thiophene in the NDI-arylene copolymer backbone does not significantly modify the electronic structure. We note that this result is very different from comparison between NDI-arylene copolymers containing biselenophene and bithiophene, where large differences in electronic structure, optical bandgap, and electron mobility were observed due to enhanced intramolecular charge transfer effects in favor of the NDI-biselenophene copolymer.^{7,46}

The thin-film absorption spectrum and the HOMO/LUMO energy levels for the donor polymer PBDB-T are also shown in Figure 1b and 1c, respectively. Although the optical bandgap (E_g^{opt}) of PBDB-T $(\sim 1.8 \text{ eV})^{49,50}$ is slightly larger than those of the acceptor polymers, there is a large spectral overlap between PBDB-T and both acceptor polymers (Figure 1b). The lack of complementary absorption among PBDB-T and PNDIT-hd or PNDIS-hd means that their binary blends are not ideal for the broader coverage of solar light harvesting. Furthermore, the absorption coefficient of PBDB-T (1.78 × 10⁵ cm⁻¹) is much higher than that of either PNDIT-hd (0.58 \times 10⁵ cm⁻¹) or PNDIS-hd (0.5 \times 10⁵ cm⁻¹). The HOMO/ LUMO energy levels for PBDB-T are -5.33/-2.92 eV.50 Thus, the offset of the HOMO levels (Δ HOMO) in the PBDB-T:PNDIT-hd and PBDB-T:PNDIS-hd binary blends is 0.93–0.95 eV, and the offset of the LUMO levels (Δ LUMO) is 0.62-0.63 eV (Figure 1c), ensuring sufficiently large driving forces for efficient electron and hole transfer processes and overall charge separation.5

Photovoltaic Properties. We fabricated and evaluated all-PSCs with an inverted device structure: ITO/ZnO(PEI)/blend/MoO₃ (0.5 nm)/Ag (100 nm). The blend composition in terms of the donor:acceptor (D:A) ratio and the active layer processing conditions, including the concentration of any processing additive, film thickness, annealing temperature, and duration of annealing, were varied and optimized to achieve the best performance for each blend system (Tables S2–S4). The optimal D:A ratio was found to be 1:1.25 (w/w) for both PBDB-T:PNDIT-hd and PBDB-T:PNDIS-hd bends. The optimal annealing temperatures were 155 °C for PBDB-T:PNDIT-hd and 135 °C for PBDB-T:PNDIS-hd, and the optimal thicknesses were found to be 90–100 nm. The photovoltaic device parameters of the optimized all-PSCs under different processing conditions are summarized in Table

The optimized PNDIT-hd:PBDB-T all-PSCs, fabricated without using any processing additive, achieved a maximum PCE of 6.52% with $J_{\rm sc}=11.45~{\rm mA/cm^2},~V_{\rm oc}=0.83~{\rm V}$ and a high FF of 0.68. The similarly fabricated PNDIS-hd:PBDB-T blend all-PSCs afforded a much higher efficiency of 8.01% PCE with $J_{\rm sc}=14.29~{\rm mA/cm^2},~V_{\rm oc}=0.82~{\rm V}$, and equally high FF of 0.68. The similarity of the $V_{\rm oc}$ of both PNDIS-hd and PNDIT-hd all-PSCs is in excellent agreement with their identical electronic structures or HOMO/LUMO energy levels. It is

clear that the primary effect of the selenophene substitution on the photovoltaic properties is the substantial enhancement in photocurrent and thus efficiency of PNDIS-hd blends because both the photovoltage and fill factor are identical in both PNDIT-hd and PNDIS-hd blend devices. The origin of the large difference in photocurrent is not obvious given that both PNDIT-hd and PNDIS-hd have very similar optical absorption bands and thus light-harvesting properties; we will seek to elucidate the origin of this difference through studies of blend photophysics, blend morphology, and charge transport in active layers discussed below.

The addition of an optimal amount of a processing additive, diphenyl ether (DPE), during the solution processing of the active layers in the all-PSCs was explored as a way to further improve the performance of each binary blend system. The J-V curves of PBDB-T:PNDIT-hd and PBDB-T:PNDIS-hd all-PSCs fabricated by means of a DPE-processing additive are presented in Figure 2a, and the photovoltaic parameters are

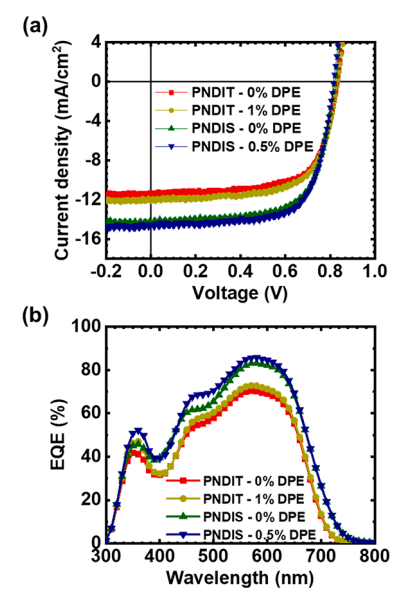


Figure 2. J-V curves (a) and EQE profiles (b) for PNDIT-hd:PBDB-T and PNDIS-hd:PBDB-T all-PSCs fabricated without and with DPE processing additive.

summarized in Table 1. PNDIT-hd: PBDB-T blends processed with an optimum 1% (v/v) DPE additive showed the best PCE of 6.74% with a $J_{\rm sc}=12.18$ mA/cm², $V_{\rm oc}=0.83$ V, and FF = 0.66. Compared to the corresponding PNDIT-hd:PBDB-T blends processed without an additive, there is only a marginal improvement in performance due to a small increase in $J_{\rm sc}$, a small decrease in FF, and a constant $V_{\rm oc}$. We found that the addition of an optimum 0.5% (v/v) DPE processing additive during the fabrication of PNDIS-hd:PBDB-T all-PSCs similarly resulted in only marginal improvement in efficiency to 8.36% PCE with $J_{\rm sc}=14.50$ mA/cm², $V_{\rm oc}=0.82$ V, and FF = 0.71

relative to devices processed without an additive. Here too, the photovoltage was unchanged, but small increases in $J_{\rm sc}$ and fill factor account for the observed increase in overall efficiency. Overall, these results clearly show that all-PSCs based on blends of the selenophene-containing acceptor PNDIS-hd are far superior to those based on similar blends of the thiophene-containing acceptor polymer PNDIT-hd, with or without the use of a processing additive in the fabrication of the active layers.

Figure 2b shows the EQE spectra corresponding to the optimal all-PSCs devices whose I-V curves are plotted in Figure 2a. The photoresponse of the PNDIT-hd:PBDB-T blends turns on at \sim 740 nm and extends to 300 nm, showing a narrow EQE peak of 70-73% at 560-580 nm. The EQE value drops significantly to only ~40% in the 350-450 nm range. The EQE spectra of the PNDIS-hd:PBDB-T blend devices are slightly broader than those of PNDIT-hd:PBDB-T blend devices, turning on at ~750 nm. Notably, the EQE of the PNDIS-hd-based all-PSCs have maximum values (EQE_{max}) that are significantly higher at 83-86%, with or without the use of a DPE processing additive. The much higher EQE values exhibited by the PNDIS-hd:PBDB-T blend devices at all wavelengths compared to the PNDIT-hd:PBDB-T blend devices clearly suggest far more efficient charge generation, dissociation, and collection in the selenophene-containing blend system. We note that the integrated EQE spectra gave calculated J_{sc} values (Table 1) that are within experimental errors (<2-5%) of those measured directly from the J-Vcurves.

We highlight the quite high fill factors observed in the present PNDIT-hd and PNDIS-hd-based all-PSCs since low FF has long been considered a major drawback of all-PSCs, and this has been hypothesized to be largely due to nonoptimal blend morphology and associated effects on poor charge generation or transport. For example, only a small number of all-PSCs have been reported with fill factors of 0.70 or higher, ^{24,48,58-63} and most of those high FF devices have been achieved via terpolymer ^{58,61,63} or ternary blend ^{58,59,61,62} strategies, and largely involved the well-studied acceptor polymer, N2200. In the present PNDIT-hd:PBDB-T and PNDIS-hd:PBDB-T all-PSC devices, FF values of 0.66-0.68 were obtained without the use of a processing additive in fabricating the active layers; the FF values of the all-PSCs reach 0.68-0.71 by using a DPE processing additive. These fill factor values are the highest observed to date for all-PSCs based on either PNDIT-hd $^{56,64-66}$ or PNDIS-hd $^{6,9,56,65,67-70}$ as the acceptor polymer. The present high fill factors achieved for PNDIT-hd:PBDB-T and PNDIS-hd:PBDB-T all-PSC devices demonstrate that FF is not determined solely by either the acceptor or the donor component but rather by a suitable combination of both, leading to an optimal blend morphology and associated blend photophysics and charge transport and collection.

Exciton Dissociation and Charge Collection. We measured the photocurrent density $(J_{\rm ph})$ versus the effective voltage $(V_{\rm eff})$ to evaluate the extent of exciton dissociation and charge collection 71,72 in the present PNDIT-hd:PBDB-T and PNDIS-hd:PBDB-T all-PSCs. Figure 3a shows a plot of $J_{\rm ph}=J_{\rm L}-J_{\rm D}$, where $J_{\rm L}$ and $J_{\rm D}$ stand for current densities under illumination and in the dark, respectively, versus $V_{\rm eff}=V_{\rm bi}-V_{\rm appl}$, where $V_{\rm bi}$ is the built-in voltage at $J_{\rm ph}=0$, and the $V_{\rm appl}$ is the applied voltage. It is seen that the $J_{\rm ph}$ reaches a plateau at $V_{\rm eff}$ of 0.5 V in all four blend systems, indicating that free

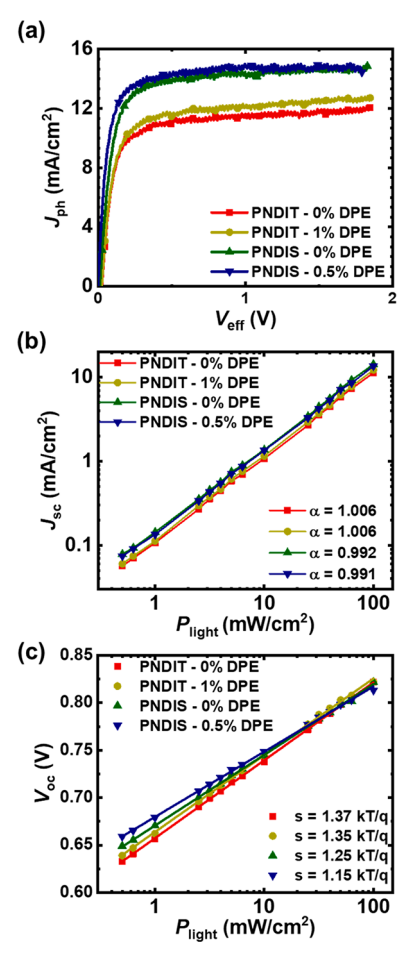


Figure 3. $J_{\rm ph}-V$ curves (a), $J_{\rm sc}$ versus light intensity (b), and $V_{\rm oc}$ versus light intensity (c) for optimized PNDIT-hd:PBDB-T and PNDIS-hd:PBDB-T blend films processed without and with DPE additive.

charge carriers generated in the all-PSCs are rapidly swept out. Thus, there appears to be no difference between the PNDIT-hd and PNDIS-hd devices or between those fabricated with or without the use of a processing additive.

The charge collection probability P(E, T) at short-circuit condition, estimated as the ratio $J_{\rm sc}/J_{\rm sat}$, where $J_{\rm sat}$ the saturated $J_{\rm ph}$ value at high $V_{\rm eff}$, was found to be generally high at 94.0% for PNDIT-hd:PBDB-T and 96.2% for PNDIS-hd:PBDB-T devices processed without the use of a processing additive. The corresponding PNDIT-hd and PNDIS-hd all-PSCs processed by using a DPE processing additive were only marginally higher with P(E, T) of 94.8% and 96.5%, respectively. We conclude that the observed large difference in the photovoltaic properties of PNDIT-hd and PNDIS-hd does not originate from a significant difference in the charge dissociation and collection processes.

Charge Recombination. The dependence of photocurrent $(J_{\rm sc})$ on the incident light intensity $(P_{\rm in})$ was measured to examine the bimolecular recombination within the all-PSC devices. Generally, in polymer solar cells, the dependence of $J_{\rm sc}$ on $P_{\rm in}$ is expected to follow a power-law relationship: $J_{\rm sc} \propto P_{\rm in}{}^{\alpha}$, where significant deviation of the exponent from unity $(\alpha = 1)$ is considered to arise from bimolecular recombination. As shown in Figure 3b and Table 2, all four all-PSCs based on PNDIT-hd and PNDIS-hd, regardless of the processing strategy, follow the power-law behavior exactly with α values

Table 2. Charge Dissociation and Recombination Parameters, Ideality Factor, and Carrier Mobilities for PNDIT-hd:PBDB-T and PNDIS-hd:PBDB-T Devices

blend	DPE (%)	P(E,T) (%)	α	s (kT/q)	$\mu_{\rm e}~(\times 10^{-5}~{\rm cm}^2{\rm V}^{-1}{\rm s}^{-1})$	$\mu_{\rm h}~(\times 10^{-4}~{\rm cm}^2{\rm V}^{-1}{\rm s}^{-1})$	$\mu_{ m h}/\mu_{ m e}$
PNDIT-hd		94.0	1.006	1.37	$2.15 \ (1.62 \pm 0.64)$	$4.23 (3.74 \pm 0.33)$	23.1
PNDIT-hd	1	94.8	1.006	1.35	$3.76 (3.11 \pm 0.53)$	$6.46 (5.92 \pm 0.64)$	19.0
PNDIS-hd		96.2	0.992	1.25	$2.43 (1.77 \pm 0.51)$	$4.98 (4.04 \pm 0.66)$	22.8
PNDIS-hd	0.5	96.5	0.991	1.15	$3.17 (3.07 \pm 0.80)$	$5.62 (5.20 \pm 0.48)$	16.9

of 0.991-1.006. These results indicate that bimolecular recombination loss mechanism is negligible at short circuit condition in these all-PSCs and is thus not the limiting factor for their photovoltaic performance. We evaluated the dependence of V_{oc} on the light intensity $(P_{in})^{73-75}$ and calculated the ideality factor $s = \frac{kT}{q} \frac{\partial V_{\text{oc}}}{\partial \ln(P_{\text{in}})}$ toward examination of monomolecular recombination as a loss mechanism in the present all-PSCs. An ideality factor of unity (s = kT/q) implies that bimolecular recombination is predominant at open circuit condition, while an s value approaching 2kT/q signifies that monomolecular or trap-assisted recombination loss dominates. From the slopes extracted from Figure 3c and presented in Table 2, we found that the ideality values of PNDIS-hd devices are much closer to unity than those for PNDIT-hd devices $(1.37 \ kT/q \ \text{and} \ 1.35 \ kT/q)$, suggesting that monomolecular recombination loss is less severe in the former devices than the PNDIT-hd all-PSCs.

Charge Transport Properties. We examined the extent that charge transport limits the performance of these PNDIT-hd and PNDIS-hd blend devices and contributes to explanation of the observed differences in photovoltaic properties by investigating single-carrier devices. The hole-and electron-only devices, analyzed by the space-charge-limited current (SCLC) method, were fabricated with the architectures: ITO/PEDOT:PSS/active layer/MoO₃/Ag (hole-only) and ITO/ZnO(PEI)/active layer/LiF/Al (electron-only), where PEDOT:PSS is the hole injection layer and ZnO(PEI) is the electron injection layer. The $J^{1/2}$ –V characteristics of single-carrier devices are presented in Figures S6 and S7, and the calculated carrier mobilities are summarized in Table 2.

The hole mobility (μ_h) varied from $4.2 \times 10^{-4} \text{ cm}^2 \text{V}^{-1} \text{s}^{-1}$ in the optimal PNDIT-hd:PBDB-T blend devices processed without using a processing additive to $5.0 \times 10^{-4} \text{ cm}^2 \text{V}^{-1} \text{s}^{-1}$ in the corresponding PNDIS-hd:PBDB-T devices. The use of a DPE processing additive resulted in the hole mobility improving slightly to $\sim 6 \times 10^{-4} \text{ cm}^2 \text{V}^{-1} \text{s}^{-1}$ in both PNDIThd:PBDB-T blend devices and PNDIS-hd:PBDB-T devices. The observed hole mobility in the present all-PSC devices is comparable to that in other reported PBDB-T-based all-PSC devices. 7,15,25,76 However, the electron mobility (μ_e) varied from 2.2×10^{-5} cm²V⁻¹s⁻¹ in the PNDIT-hd devices to $2.4 \times$ $10^{-5} \text{ cm}^2 \text{V}^{-1} \text{s}^{-1}$ in PNDIS-hd devices processed without using a processing additive. The electron mobility in devices processed by using a DPE processing additive slightly improved to 3.8×10^{-5} and 3.2×10^{-5} cm²V⁻¹s⁻¹ in the PNDIT-hd and PNDIS-hd devices, respectively. Among the striking features of these results include the fact that electron transport is not significantly different among the all-PSCs based on the two different acceptor polymers. Charge transport in all the present all-PSCs is highly asymmetric with the μ_h/μ_e ratios varying from 23 in the devices fabricated without the use of a processing additive to below 17-19 in devices produced with the aid of a DPE processing additive

(Table 2). Despite the large asymmetry in the charge transport properties of both PNDIT-hd:PBDB-T and PNDIS-hd:PBDB-T blend devices, the observed high fill factors of 0.68–0.71 suggest that the all-PSCs have favorable morphology that enabled efficient charge photogeneration and collection.

We conclude that poor electron transport is an important limitation of the present all-PSC devices based on both PNDIT-hd and PNDIS-hd acceptor polymers. On the other hand, the slightly different electron mobilities in the all-PSCs based on PNDIT-hd and PNDIS-hd could not account for the observed large difference in photovoltaic properties discussed earlier.

Blend Surface Morphology. AFM imaging was used to characterize the surface morphology of the optimal PNDIT-hd:PBDB-T and PNDIS-hd:PBDB-T all-PSC devices. The height and phase images of the PNDIT-hd:PBDB-T blend films processed without and with DPE additive are presented in Figure 4a and 4b, respectively. The height and phase images of the PNDIS-hd:PBDB-T blend films processed without and with DPE additive are presented in Figure 4c and 4d, respectively.

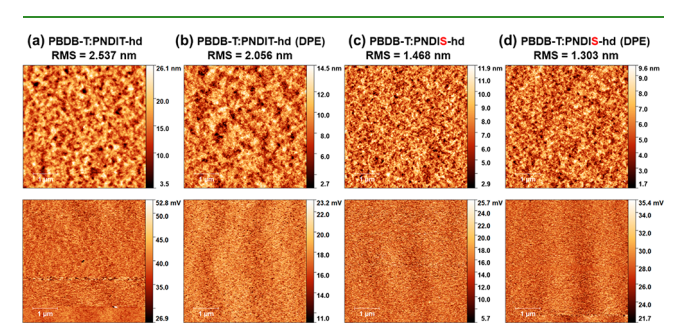


Figure 4. AFM height and phase images $(5 \times 5 \mu m)$ of polymer blends: (a) PBDB-T:PNDIT-hd, (b) PBDB-T:PNDIS-hd, (c) PBDB-T:PNDIT-hd processed with 1% DPE, and (d) PBDB-T:PNDIS-hd films processed with 0.5% DPE.

The most striking feature of these images of the surface morphology of the all-PSCs is the large difference between blend films containing the two different acceptor polymers PNDIT-hd and PNDIS-hd. Blend films containing the thiophene-linked acceptor polymer, PNDIT-hd, generally showed a much coarser surface morphology with larger domains than those containing the selenophene-linked acceptor polymer, PNDIS-hd. The surface roughness as measured by the root-mean-square (RMS) value for PNDIT-hd:PBDB-T blend films was 2.5 nm without using a processing additive and 2.1 nm for the corresponding active layers processed with aid of a DPE additive. In contrast, the RMS value for PNDIShd:PBDB-T blend films processed without using a processing additive was 1.5 nm, which decreases to 1.3 nm when a DPE processing additive was used in fabricating the active layer. It is also clear that the use of the DPE processing additive in

processing the active layer does lead to a smaller (\sim 13–16%) decrease in the surface roughness.

The surface morphology of PNDIS-hd:PBDB-T blend films processed without and with DPE additive (Figure 4c, 4d) shows relatively uniform fine scale features across the whole surface area, indicating good intermixing between the donor and acceptor polymers with no obvious large scale phase separation. In the case of PNDIT-hd:PBDB-T blend films processed with DPE additive (Figure 4b), some fibril-like patterns are visible, whereas apparent larger scale phaseseparated microstructure is seen in the corresponding blend films processed without DPE additive (Figure 4a). The fine scale microstructures observed in the surface morphology of PNDIS-hd:PBDB-T blend films are consistent with the enhanced photovoltaic properties compared to PNDIThd:PBDB-T blend films. We conclude that the molecularlevel substitution of selenophene for thiophene in the polymer backbone when going from PNDIT-hd to PNDIS-hd has resulted in a significant and beneficial change in the blend film surface morphology than what could be achieved by the use of a processing additive.

Bulk Blend Morphology. We used grazing-incidence wide-angle X-ray scattering (GIWAXS) measurements to characterize the thin-film microstructures of the two pristine acceptor polymers, PNDIT-hd and PNDIS-hd, and their binary blends with the donor polymer, PBDB-T. The GIWAXS investigation was focused on the pristine and blend thin films processed under the conditions used in fabricating the optimal all-PSCs without the use of a processing additive; as discussed earlier, only marginal changes in the blend photophysics, charge photogeneration and recombination dynamics, and photovoltaic properties were observed by using a DPE processing additive in fabricating devices. The 2D-GIWAXS images and the corresponding line cuts for the neat acceptor polymer films are presented in Figure 5. A schematic illustration of the molecular packing of PNDIT-hd and PNDIS-hd, and the relevant d-spacings, is shown in Figure S8. The peak positions, d-spacings, and the crystalline

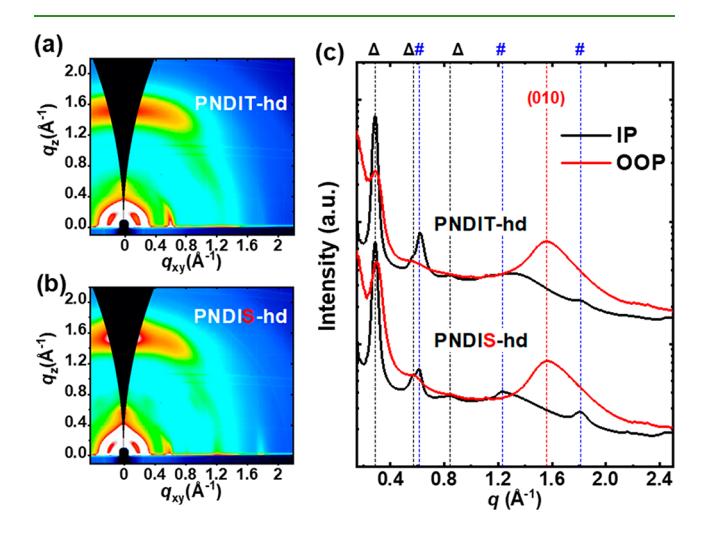


Figure 5. 2D GIWAXS characterization of pristine acceptor polymer thin films: (a) 2D GIWAXS pattern of PNDIT-hd; (b) 2D GIWAXS pattern of PNDIS-hd; and (c) line-cut profiles for pristine films of PNDIT-hd and PNDIS-hd. " Δ " denotes the in-plane lamellar diffraction peaks (100) (200) (300), and "#" denotes the (001), (002), and (003) diffraction peaks of the backbone ordering.

coherence length (L_c) for the neat polymer films are summarized in Table 3. The 2D-GIWAXS images and the corresponding line cuts for the neat donor polymer film and the photovoltaic blend films are shown in Figure 6.

Table 3. Summary of In-Plane (IP) and Out-of-Plane (OOP) Peaks from 2D GIWAXS Data on Polymer and Blend Thin Films

		IP (100)		OOP (010)			
polymer	q_{xy} (A^{xy})	d-spacing (Å)	$L_{\rm c} m (nm)$	q_{z} (\mathring{A}^{-1})	d-spacing (Å)	L _c (nm)	
PBDB-T	0.290	21.69	7.01	1.68	3.74	1.47	
PNDIT-hd	0.285	22.05	14.68	1.57	4.00	1.13	
PNDIS-hd	0.288	21.85	17.31	1.59	3.94	1.60	
PNDIT-hd: PBDB-T	0.287	21.91	10.94	1.63	3.86	1.40	
PNDIS-hd: PBDB-T	0.286	21.96	11.26	1.62	3.87	1.38	

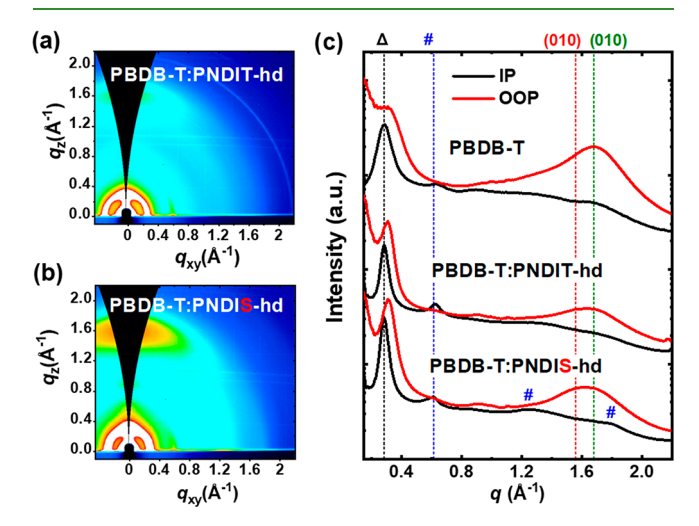


Figure 6. 2D GIWAXS characterizations of polymer blend thin films: (a) 2D GIWAXS image for PBDB-T:PNDIT-hd blend, (b) 2D GIWAXS image for PBDB-T:PNDIS-hd blend, and (c) line-cut profiles for pristine PBDB-T and its blends with PNDIT-hd and PNDIS-hd, respectively. " Δ " denotes the in-plane lamellar diffraction peak (100), and "#" denotes the diffraction peaks for the backbone ordering (001). The π - π stacking peak (010) positions from PBDB-T and PNDIT-hd and PNDIS-hd are also marked.

Neat films of both PNDIT-hd and PNDIS-hd exhibit intense (100) diffraction peaks in the in-plane (IP) direction (q_{xy} = $0.285-0.290 \text{ Å}^{-1}$), corresponding to d-spacing values of 21.7-22.1 Å (Table 3). The comparable lamellar stacking distance observed in PNDIT-hd and PNDIS-hd is consistent with their similar molecular structures. Higher order in-plane diffraction peaks (200) (q_{xy} = 0.56 Å $^{-1}$) and (300) (q_{xy} = 0.84 Å $^{-1}$) were also observed in both neat PNDIT-hd and PNDIS-hd films (Figure 5c), suggesting the highly crystalline and well-ordered nature of the acceptor polymer chains.⁷⁷ Additionally, the (001) diffraction peaks in the IP direction were present in both acceptor polymer films at q_{xy} of 0.61–0.62 Å⁻¹, which suggest strong ordering along the polymer backbone directions. The dspacing values for the IP (001) peaks are found to be 10.13 and 10.30 Å for PNDIT-hd and PNDIS-hd, respectively, where the larger d-spacing of PNDIS-hd can be explained by the slightly larger molecular width of the selenophene ring relative to the thiophene ring.

In the out-of-plane (OOP) direction, the neat PNDIT-hd and PNDIS-hd films showed pronounced and broad (010) diffraction peaks with comparable intensity at q_z of 1.57 and 1.59 Å⁻¹ corresponding to a π - π stacking distance of 4.00 and 3.94 Å (Table 3), respectively. Compared to PNDIT-hd, PNDIS-hd exhibited a much more intense (100) diffraction peak in the OOP direction (Figure S9b). Thus, the coexistence of the pronounced IP (100) peak and the distinct OOP (100) and (010) peaks in the PNDIS-hd films suggest that PNDIShd had mixed face-on and edge-on oriented crystallites, whereas PNDIT-hd showed preferentially face-on molecular orientations. The crystalline coherence length (L_c) values estimated by using the Scherrer equation⁷⁸ are presented in Table 3. The $L_{\rm c}$ values of PNDIS-hd calculated from the IP (100) and OOP (010) peaks were found to be higher than those of PNDIT-hd (Table 3), indicating that PNDIS-hd has enhanced crystallinity in both the lamellar and $\pi - \pi$ stacking directions.

As shown in Figure 6c, the neat donor polymer PBDB-T films exhibit intense (100) diffraction and (010) diffraction peaks in the IP and OOP directions at q_{xy} of 0.29 Å $^{-1}$ and q_z of 1.68 Å $^{-1}$, respectively, suggesting that PBDB-T exhibited predominantly *face-on* orientated crystallites. The $L_{\rm c}$ of neat PBDB-T films was found to be 7.01 nm (Table 3). The 2D-GIWAXS results for the donor polymer PBDB-T agree well with previous reports. 7,76

The (010) diffraction peaks in the OOP directions of both blend films are broadened and centered at q_z values that lied between the q_z of the donor and acceptor polymers (Table 3), which indicates that there is intimate mixing between the donor and acceptor polymers. As shown in Figure 6b, distinct and bright OOP (010) diffraction patterns are present in the PNDIS-hd:PBDB-T blends, whereas the PNDIT-hd:PBDB-T blends showed minimal diffraction patterns in the OOP direction (Figure 6a). This result argues that the populations of face-on oriented crystallites are significantly higher in the PNDIS-hd:PBDB-T blends. The PNDIT-hd:PBDB-T blends were also found to exhibit increased populations of edge-on oriented crystallites compared to either of the neat component polymers as evidenced by the enhanced intensity of the (100) diffraction peak in the OOP direction (Figure S10e). The coexistence of face-on and edge-on oriented crystallites in PNDIT-hd:PBDB-T blends could justify the poorer photovoltaic properties as discussed above. The larger L_c value of the PNDIS-hd:PBDB-T blend films ($L_c = 11.26$ nm) suggest enhanced crystallinity compared to that of the thiophenecontaining blend counterparts ($L_c = 10.94$ nm). Overall, these 2D-GIWAXS results and analysis collectively demonstrate that compared to the PNDIT-hd blend counterparts, PNDIShd:PBDB-T blends have a more optimal blend morphology that features predominantly face-on oriented crystallites with enhanced blend crystallinity; thus, corroborating the observed enhanced photovoltaic properties.

CONCLUSIONS

In summary, we used the alternating naphthalene diimide-thiophene copolymer, PNDIT-hd, and naphthalene diimide-selenophene copolymer, PNDIS-hd, to investigate the effects of the donor moiety substitution on the intrinsic and photovoltaic blend properties of n-type semiconducting copolymers with simple donor—acceptor structure. Although both PNDIT-hd and PNDIS-hd have identical electrochemically derived HOMO/LUMO energy levels, we found that the latter acceptor polymer has a broadened optical absorption

with an optical bandgap of 1.70 eV, which is 0.07 eV narrower relative to PNDIT-hd. In binary blends with the donor polymer PBDB-T, the selenophene-containing acceptor polymer PNDIS-hd enabled all-PSCs with significantly enhanced photocurrent, EQE, and overall photovoltaic power conversion efficiency compared to the thiophene-containing acceptor polymer. PNDIT-hd:PBDB-T-based all-PSCs could thus achieve a PCE of 6.7% ($J_{sc} = 12.18 \text{ mA/cm}^2$, FF = 0.66), whereas the corresponding PNDIS-hd:PBDB-T devices showed a higher PCE of 8.4% (J_{sc} = 14.50 mA/cm², FF = 0.71). The observed enhanced photovoltaic properties of the selenophene-containing polymer PNDIS-hd could largely be accounted for by its improved light harvesting, formation of optimal blend morphology as evidenced by the 2D GIWAXS results, and reduced monomolecular recombination losses, compared to its thiophene counterpart, PNDIT-hd. These results demonstrate the many advantages in selenophene substitution for thiophene in the design of n-type semiconducting polymers with donor-acceptor architectures for applications in all-polymer solar cells.

ASSOCIATED CONTENT

Supporting Information

The Supporting Information is available free of charge at https://pubs.acs.org/doi/10.1021/acsapm.0c00772.

Additional characterization data, including ^{1}H NMR spectra, TGA, DSC, UV-vis, CV, $J^{0.5}-V$ measurement by SCLC and the corresponding fits, 2D-GIWAXS line cuts of neat polymers and blend films, and details of device optimization (PDF)

AUTHOR INFORMATION

Corresponding Author

Samson A. Jenekhe — Department of Chemical Engineering and Department of Chemistry, University of Washington, Seattle, Washington 98195-1750, United States; orcid.org/0000-0002-0898-9541; Email: jenekhe@u.washington.edu

Authors

Xiaomei Ding — Department of Chemical Engineering and Department of Chemistry, University of Washington, Seattle, Washington 98195-1750, United States; orcid.org/0000-0001-8147-3149

Duyen K. Tran – Department of Chemical Engineering and Department of Chemistry, University of Washington, Seattle, Washington 98195-1750, United States; ○ orcid.org/0000-0002-3065-6153

Daiki Kuzuhara — Faculty of Science and Engineering, Iwate University, Morioka, Iwate 020-8551, Japan; ocid.org/0000-0001-7948-8501

Tomoyuki Koganezawa – Industrial Application Division, Japan Synchrotron Radiation Research Institute, Sayo, Hyogo 679-5198, Japan

Complete contact information is available at: https://pubs.acs.org/10.1021/acsapm.0c00772

Notes

The authors declare no competing financial interest.

ACKNOWLEDGMENTS

This work was supported by the NSF (DMR-1708450) and in part by the Office of Naval Research (N00014-17-1-2203).

D.K.T. gratefully acknowledges the University of Washington Clean Energy Institute Fellowship. The synchrotron radiation-based 2D-GIWAXS experiments were performed at the BL46XU of SPring-8 with the support of the Japan Synchrotron Radiation Research Institute (JASRI) (Proposal 2018A1744).

REFERENCES

- (1) Lee, C.; Lee, S.; Kim, G. U.; Lee, W.; Kim, B. J. Recent Advances, Design Guidelines, and Prospects of All-Polymer Solar Cells. *Chem. Rev.* **2019**, *119*, 8028–8086.
- (2) Wang, G.; Melkonyan, F. S.; Facchetti, A.; Marks, T. J. All-Polymer Solar Cells: Recent Progress, Challenges, and Prospects. *Angew. Chem., Int. Ed.* **2019**, 58, 4129–4142.
- (3) Genene, Z.; Mammo, W.; Wang, E.; Andersson, M. R. Recent Advances in n-Type Polymers for All-Polymer Solar Cells. *Adv. Mater.* **2019**, *31*, 1807275.
- (4) Benten, H.; Mori, D.; Ohkita, H.; Ito, S. Recent research progress of polymer donor/polymer acceptor blend solar cells. *J. Mater. Chem. A* **2016**, *4*, 5340–5365.
- (5) Facchetti, A. Polymer donor-polymer acceptor (all-polymer) solar cells. *Mater. Today* **2013**, *16*, 123–132.
- (6) Earmme, T.; Hwang, Y. J.; Murari, N. M.; Subramaniyan, S.; Jenekhe, S. A. All-polymer solar cells with 3.3% efficiency based on naphthalene diimide-selenophene copolymer acceptor. *J. Am. Chem. Soc.* **2013**, *135*, 14960–14963.
- (7) Kolhe, N. B.; Lee, H.; Kuzuhara, D.; Yoshimoto, N.; Koganezawa, T.; Jenekhe, S. A. All-Polymer Solar Cells with 9.4% Efficiency from Naphthalene Diimide-Biselenophene Copolymer Acceptor. *Chem. Mater.* **2018**, *30*, 6540–6548.
- (8) Hwang, Y. J.; Earmme, T.; Courtright, B. A.; Eberle, F. N.; Jenekhe, S. A. n-Type semiconducting naphthalene diimide-perylene diimide copolymers: controlling crystallinity, blend morphology, and compatibility toward high-performance all-polymer solar cells. *J. Am. Chem. Soc.* **2015**, 137, 4424–4434.
- (9) Hwang, Y. J.; Courtright, B. A.; Ferreira, A. S.; Tolbert, S. H.; Jenekhe, S. A. 7.7% Efficient All-Polymer Solar Cells. *Adv. Mater.* **2015**, *27*, 4578–4584.
- (10) Yao, H.; Bai, F.; Hu, H.; Arunagiri, L.; Zhang, J.; Chen, Y.; Yu, H.; Chen, S.; Liu, T.; Lai, J. Y. L.; Zou, Y.; Ade, H.; Yan, H. Efficient All-Polymer Solar Cells based on a New Polymer Acceptor Achieving 10.3% Power Conversion Efficiency. ACS Energy Lett. 2019, 4, 417–422.
- (11) Tran, D. K.; Kolhe, N. B.; Hwang, Y. J.; Kuzuhara, D.; Koganezawa, T.; Jenekhe, S. A. Effects of a Fluorinated Donor Polymer on the Morphology, Photophysics, and Performance of All-Polymer Solar Cells Based on Naphthalene Diimide-Arylene Copolymer Acceptors. ACS Appl. Mater. Interfaces 2020, 12, 16490–16502.
- (12) Wang, W.; Wu, Q.; Sun, R.; Guo, J.; Wu, Y.; Shi, M.; Yang, W.; Li, H.; Min, J. Controlling Molecular Mass of Low-Band-Gap Polymer Acceptors for High-Performance All-Polymer Solar Cells. *Joule* **2020**, *4*, 1070–1086.
- (13) Fan, Q.; Su, W.; Chen, S.; Kim, W.; Chen, X.; Lee, B.; Liu, T.; Méndez-Romero, U. A.; Ma, R.; Yang, T.; Zhuang, W.; Li, Y.; Kim, T.-S.; Hou, L.; Yang, C.; Yan, H.; Yu, D.; Wang, E. Mechanically Robust All-Polymer Solar Cells from Narrow Band Gap Acceptors with Hetero-Bridging Atoms. *Joule* **2020**, *4*, 658–672.
- (14) Feng, K.; Huang, J.; Zhang, X.; Wu, Z.; Shi, S.; Thomsen, L.; Tian, Y.; Woo, H. Y.; McNeill, C. R.; Guo, X. High-Performance All-Polymer Solar Cells Enabled by n-Type Polymers with an Ultranarrow Bandgap Down to 1.28 eV. *Adv. Mater.* **2020**, 32, 2001476.
- (15) Lee, J. W.; Sung, M. J.; Kim, D.; Lee, S.; You, H.; Kim, F. S.; Kim, Y. H.; Kim, B. J.; Kwon, S. K. Naphthalene Diimide-Based Terpolymers with Controlled Crystalline Properties for Producing High Electron Mobility and Optimal Blend Morphology in All-Polymer Solar Cells. *Chem. Mater.* **2020**, *32*, 2572–2582.

- (16) Xie, B.; Zhang, K.; Hu, Z.; Fang, H.; Lin, B.; Yin, Q.; He, B.; Dong, S.; Ying, L.; Ma, W.; Huang, F.; Yan, H.; Cao, Y. Polymer Pre-Aggregation Enables Optimal Morphology and High Performance in All-Polymer Solar Cells. *Solar RRL* **2020**, *4*, 1900385.
- (17) Fan, Q.; Ma, R.; Liu, T.; Su, W.; Peng, W.; Zhang, M.; Wang, Z.; Wen, X.; Cong, Z.; Luo, Z.; Hou, L.; Liu, F.; Zhu, W.; Yu, D.; Yan, H.; Wang, E. 10.13% Efficiency All-Polymer Solar Cells Enabled by Improving the Optical Absorption of Polymer Acceptors. *Solar RRL* **2020**, *4*, 2000142.
- (18) Du, J.; Hu, K.; Meng, L.; Angunawela, I.; Zhang, J.; Qin, S.; Liebman-Pelaez, A.; Zhu, C.; Zhang, Z.; Ade, H.; Li, Y. High-Performance All-Polymer Solar Cells: Synthesis of Polymer Acceptor by a Random Ternary Copolymerization Strategy. *Angew. Chem. Int. Ed.* **2020**, *59*, 15181–15185.
- (19) Yao, H.; Ma, L.-K.; Yu, H.; Yu, J.; Chow, P. C. Y.; Xue, W.; Zou, X.; Chen, Y.; Liang, J.; Arunagiri, L.; Gao, F.; Sun, H.; Zhang, G.; Ma, W.; Yan, H. All-Polymer Solar Cells with over 12% Efficiency and a Small Voltage Loss Enabled by a Polymer Acceptor Based on an Extended Fused Ring Core. *Adv. Energy Mater.* **2020**, 2001408.
- (20) Jia, T.; Zhang, J.; Zhong, W.; Liang, Y.; Zhang, K.; Dong, S.; Ying, L.; Liu, F.; Wang, X.; Huang, F.; Cao, Y. 14.4% efficiency all-polymer solar cell with broad absorption and low energy loss enabled by a novel polymer acceptor. *Nano Energy* **2020**, *72*, 104718.
- (21) Kim, W.; Choi, J.; Kim, J.-H.; Kim, T.; Lee, C.; Lee, S.; Kim, M.; Kim, B. J.; Kim, T.-S. Comparative Study of the Mechanical Properties of All-Polymer and Fullerene—Polymer Solar Cells: The Importance of Polymer Acceptors for High Fracture Resistance. *Chem. Mater.* **2018**, *30*, 2102–2111.
- (22) Kim, T.; Kim, J. H.; Kang, T. E.; Lee, C.; Kang, H.; Shin, M.; Wang, C.; Ma, B.; Jeong, U.; Kim, T. S.; Kim, B. J. Flexible, highly efficient all-polymer solar cells. *Nat. Commun.* **2015**, *6*, 8547.
- (23) Lu, L.; Zheng, T.; Wu, Q.; Schneider, A. M.; Zhao, D.; Yu, L. Recent Advances in Bulk Heterojunction Polymer Solar Cells. *Chem. Rev.* **2015**, *115*, 12666–12731.
- (24) Gao, L.; Zhang, Z. G.; Xue, L.; Min, J.; Zhang, J.; Wei, Z.; Li, Y. All-Polymer Solar Cells Based on Absorption-Complementary Polymer Donor and Acceptor with High Power Conversion Efficiency of 8.27%. *Adv. Mater.* **2016**, *28*, 1884–1890.
- (25) Kolhe, N. B.; Tran, D. K.; Lee, H.; Kuzuhara, D.; Yoshimoto, N.; Koganezawa, T.; Jenekhe, S. A. New Random Copolymer Acceptors Enable Additive-Free Processing of 10.1% Efficient All-Polymer Solar Cells with Near-Unity Internal Quantum Efficiency. *ACS Energy Lett.* **2019**, *4*, 1162–1170.
- (26) Jenekhe, S. A.; Lu, L.; Alam, M. M. New Conjugated Polymers with Donor–Acceptor Architectures: Synthesis and Photophysics of Carbazole–Quinoline and Phenothiazine–Quinoline Copolymers and Oligomers Exhibiting Large Intramolecular Charge Transfer. *Macromolecules* **2001**, *34*, 7315–7324.
- (27) Zhu, Y.; Champion, R. D.; Jenekhe, S. A. Conjugated Donor–Acceptor Copolymer Semiconductors with Large Intramolecular Charge Transfer: Synthesis, Optical Properties, Electrochemistry, and Field Effect Carrier Mobility of Thienopyrazine-Based Copolymers. *Macromolecules* **2006**, *39*, 8712–8719.
- (28) Wu, J.-S.; Cheng, S.-W.; Cheng, Y.-J.; Hsu, C.-S. Donor–acceptor conjugated polymers based on multifused ladder-type arenes for organic solar cells. *Chem. Soc. Rev.* **2015**, *44*, 1113–1154.
- (29) Cheng, Y. J.; Yang, S. H.; Hsu, C. S. Synthesis of conjugated polymers for organic solar cell applications. *Chem. Rev.* **2009**, *109*, 5868–5923.
- (30) Guo, X.; Kim, F. S.; Seger, M. J.; Jenekhe, S. A.; Watson, M. D. Naphthalene Diimide-Based Polymer Semiconductors: Synthesis, Structure—Property Correlations, and n-Channel and Ambipolar Field-Effect Transistors. *Chem. Mater.* **2012**, *24*, 1434—1442.
- (31) Kim, F. S.; Guo, X.; Watson, M. D.; Jenekhe, S. A. Highmobility ambipolar transistors and high-gain inverters from a donor-acceptor copolymer semiconductor. *Adv. Mater.* **2010**, *22*, 478–482.
- (32) Sun, H.; Guo, X.; Facchetti, A. High-Performance n-Type Polymer Semiconductors: Applications, Recent Development, and Challenges. *Chem.* **2020**, *6*, 1310–1326.

https://dx.doi.org/10.1021/acsapm.0c00772 ACS Appl. Polym. Mater. XXXX, XXX, XXX—XXX

- (33) Sun, H.; Wang, L.; Wang, Y.; Guo, X. Imide-Functionalized Polymer Semiconductors. *Chem. Eur. J.* **2019**, *25*, 87–105.
- (34) Yang, J.; Xiao, B.; Tang, A.; Li, J.; Wang, X.; Zhou, E. Aromatic-Diimide-Based n-Type Conjugated Polymers for All-Polymer Solar Cell Applications. *Adv. Mater.* **2019**, *31*, 1804699.
- (35) Zhou, N.; Facchetti, A. Naphthalenediimide (NDI) polymers for all-polymer photovoltaics. *Mater. Today* **2018**, *21*, 377–390.
- (36) Li, H.; Kim, F. S.; Ren, G.; Hollenbeck, E. C.; Subramaniyan, S.; Jenekhe, S. A. Tetraazabenzodifluoranthene diimides: building blocks for solution-processable n-type organic semiconductors. *Angew. Chem., Int. Ed.* **2013**, 52, 5513–5517.
- (37) Li, H.; Kim, F. S.; Ren, G.; Jenekhe, S. A. High-mobility n-type conjugated polymers based on electron-deficient tetraazabenzodi-fluoranthene diimide for organic electronics. *J. Am. Chem. Soc.* **2013**, 135, 14920–14923.
- (38) Li, H.; Hwang, Y. J.; Earmme, T.; Huber, R. C.; Courtright, B. A. E.; O'Brien, C.; Tolbert, S. H.; Jenekhe, S. A. Polymer/Polymer Blend Solar Cells Using Tetraazabenzodifluoranthene Diimide Conjugated Polymers as Electron Acceptors. *Macromolecules* **2015**, 48, 1759–1766.
- (39) Fukutomi, Y.; Nakano, M.; Hu, J. Y.; Osaka, I.; Takimiya, K. Naphthodithiophenediimide (NDTI): synthesis, structure, and applications. *J. Am. Chem. Soc.* **2013**, *135*, 11445–11448.
- (40) Yang, J.; Xiao, B.; Tajima, K.; Nakano, M.; Takimiya, K.; Tang, A.; Zhou, E. Comparison among Perylene Diimide (PDI), Naphthalene Diimide (NDI), and Naphthodithiophene Diimide (NDTI) Based n-Type Polymers for All-Polymer Solar Cells Application. *Macromolecules* **2017**, *50*, 3179–3185.
- (41) Zhou, E.; Nakano, M.; Izawa, S.; Cong, J.; Osaka, I.; Takimiya, K.; Tajima, K. All-Polymer Solar Cell with High Near-Infrared Response Based on a Naphthodithiophene Diimide (NDTI) Copolymer. ACS Macro Lett. 2014, 3, 872–875.
- (42) Sun, H.; Liu, B.; Wang, Z.; Ling, S.; Zhang, Y.; Zhang, G.; Wang, Y.; Zhang, M.; Li, B.; Yang, W.; Wang, J.; Guo, H.; Liu, F.; Guo, X. Side chain engineering of polymer acceptors for all-polymer solar cells with enhanced efficiency. *J. Mater. Chem. C* **2020**, 8, 4012–4020.
- (43) Sun, H.; Tang, Y.; Koh, C. W.; Ling, S.; Wang, R.; Yang, K.; Yu, J.; Shi, Y.; Wang, Y.; Woo, H. Y.; Guo, X. High-Performance All-Polymer Solar Cells Enabled by an n-Type Polymer Based on a Fluorinated Imide-Functionalized Arene. *Adv. Mater.* **2019**, *31*, 1807220.
- (44) Wang, Y.; Guo, H.; Harbuzaru, A.; Uddin, M. A.; Arrechea-Marcos, I.; Ling, S.; Yu, J.; Tang, Y.; Sun, H.; López Navarrete, J. T.; Ortiz, R. P.; Woo, H. Y.; Guo, X. (Semi)ladder-Type Bithiophene Imide-Based All-Acceptor Semiconductors: Synthesis, Structure—Property Correlations, and Unipolar n-Type Transistor Performance. *J. Am. Chem. Soc.* **2018**, *140*, 6095–6108.
- (45) Hwang, Y. J.; Ren, G. Q.; Murari, N. M.; Jenekhe, S. A. n-Type Naphthalene Diimide-Biselenophene Copolymer for All-Polymer Bulk Heterojunction Solar Cells. *Macromolecules* **2012**, *45*, 9056–9062.
- (46) Yan, H.; Chen, Z.; Zheng, Y.; Newman, C.; Quinn, J. R.; Dötz, F.; Kastler, M.; Facchetti, A. A high-mobility electron-transporting polymer for printed transistors. *Nature* **2009**, *457*, 679–686.
- (47) Tremel, K.; Fischer, F. S. U.; Kayunkid, N.; Pietro, R. D.; Tkachov, R.; Kiriy, A.; Neher, D.; Ludwigs, S.; Brinkmann, M. Charge Transport Anisotropy in Highly Oriented Thin Films of the Acceptor Polymer P(NDI2OD-T2). *Adv. Energy Mater.* **2014**, *4*, 1301659.
- (48) Fan, B. B.; Ying, L.; Wang, Z. F.; He, B. T.; Jiang, X. F.; Huang, F.; Cao, Y. Optimisation of processing solvent and molecular weight for the production of green-solvent-processed all-polymer solar cells with a power conversion efficiency over 9%. *Energy Environ. Sci.* **2017**, 10, 1243–1251.
- (49) Qian, D. P.; Ye, L.; Zhang, M. J.; Liang, Y. R.; Li, L. J.; Huang, Y.; Guo, X.; Zhang, S. Q.; Tan, Z. A.; Hou, J. H. Design, Application, and Morphology Study of a New Photovoltaic Polymer with Strong Aggregation in Solution State. *Macromolecules* **2012**, *45*, 9611–9617.

- (50) Zhao, W.; Qian, D.; Zhang, S.; Li, S.; Inganäs, O.; Gao, F.; Hou, J. Fullerene-Free Polymer Solar Cells with over 11% Efficiency and Excellent Thermal Stability. *Adv. Mater.* **2016**, 28, 4734–4739.
- (51) Courtright, B. A.; Jenekhe, S. A. Polyethylenimine Interfacial Layers in Inverted Organic Photovoltaic Devices: Effects of Ethoxylation and Molecular Weight on Efficiency and Temporal Stability. ACS Appl. Mater. Interfaces 2015, 7, 26167–26175.
- (52) Malliaras, G. G.; Salem, J. R.; Brock, P. J.; Scott, C. Electrical characteristics and efficiency of single-layer organic light-emitting diodes. *Phys. Rev. B: Condens. Matter Mater. Phys.* **1998**, 58, R13411–R13414
- (53) Choi, J.; Kim, W.; Kim, S.; Kim, T.-S.; Kim, B. J. Influence of Acceptor Type and Polymer Molecular Weight on the Mechanical Properties of Polymer Solar Cells. *Chem. Mater.* **2019**, *31*, 9057–9069.
- (54) Zhou, N.; Dudnik, A. S.; Li, T. I. N. G.; Manley, E. F.; Aldrich, T. J.; Guo, P.; Liao, H.-C.; Chen, Z.; Chen, L. X.; Chang, R. P. H.; Facchetti, A.; Olvera de la Cruz, M.; Marks, T. J. All-Polymer Solar Cell Performance Optimized via Systematic Molecular Weight Tuning of Both Donor and Acceptor Polymers. *J. Am. Chem. Soc.* **2016**, *138*, 1240–1251.
- (55) Hwang, Y. J.; Murari, N. M.; Jenekhe, S. A. New n-type polymer semiconductors based on naphthalene diimide and selenophene derivatives for organic field-effect transistors. *Polym. Chem.* **2013**, *4*, 3187–3195.
- (56) Kim, Y.; Cho, H. H.; Kim, T.; Liao, K.; Kim, B. J. Terpolymer approach for controlling the crystalline behavior of naphthalene diimide-based polymer acceptors and enhancing the performance of all-polymer solar cells. *Polym. J.* **2016**, *48*, 517–524.
- (57) Ren, G. Q.; Schlenker, C. W.; Ahmed, E.; Subramaniyan, S.; Olthof, S.; Kahn, A.; Ginger, D. S.; Jenekhe, S. A. Photoinduced Hole Transfer Becomes Suppressed with Diminished Driving Force in Polymer-Fullerene Solar Cells While Electron Transfer Remains Active. *Adv. Funct. Mater.* **2013**, *23*, 1238–1249.
- (58) Liu, X.; Zhang, C.; Duan, C.; Li, M.; Hu, Z.; Wang, J.; Liu, F.; Li, N.; Brabec, C. J.; Janssen, R. A. J.; Bazan, G. C.; Huang, F.; Cao, Y. Morphology Optimization via Side Chain Engineering Enables All-Polymer Solar Cells with Excellent Fill Factor and Stability. *J. Am. Chem. Soc.* **2018**, *140*, 8934—8943.
- (59) Li, Z.; Ying, L.; Xie, R.; Zhu, P.; Li, N.; Zhong, W.; Huang, F.; Cao, Y. Designing ternary blend all-polymer solar cells with an efficiency of over 10% and a fill factor of 78%. *Nano Energy* **2018**, *51*, 434–441.
- (60) Fan, B.; Ying, L.; Zhu, P.; Pan, F.; Liu, F.; Chen, J.; Huang, F.; Cao, Y. All-Polymer Solar Cells Based on a Conjugated Polymer Containing Siloxane-Functionalized Side Chains with Efficiency over 10%. Adv. Mater. 2017, 29, 1703906.
- (61) Li, Z.; Xu, X.; Zhang, W.; Meng, X.; Genene, Z.; Ma, W.; Mammo, W.; Yartsev, A.; Andersson, M. R.; Janssen, R. A. J.; Wang, E. 9.0% power conversion efficiency from ternary all-polymer solar cells. *Energy Environ. Sci.* **2017**, *10*, 2212–2221.
- (62) Fan, B.; Zhu, P.; Xin, J.; Li, N.; Ying, L.; Zhong, W.; Li, Z.; Ma, W.; Huang, F.; Cao, Y. High-Performance Thick-Film All-Polymer Solar Cells Created Via Ternary Blending of a Novel Wide-Bandgap Electron-Donating Copolymer. *Adv. Energy Mater.* **2018**, *8*, 1703085.
- (63) Li, Z.; Xu, X.; Zhang, W.; Meng, X.; Ma, W.; Yartsev, A.; Inganas, O.; Andersson, M. R.; Janssen, R. A.; Wang, E. High Performance All-Polymer Solar Cells by Synergistic Effects of Fine-Tuned Crystallinity and Solvent Annealing. *J. Am. Chem. Soc.* **2016**, 138, 10935–10944.
- (64) Lee, C.; Giridhar, T.; Choi, J.; Kim, S.; Kim, Y.; Kim, T.; Lee, W.; Cho, H. H.; Wang, C.; Ade, H.; Kim, B. J. Importance of 2D Conjugated Side Chains of Benzodithiophene-Based Polymers in Controlling Polymer Packing, Interfacial Ordering, and Composition Variations of All-Polymer Solar Cells. *Chem. Mater.* **2017**, *29*, 9407–9415.
- (65) Cho, H. H.; Han, G.; Younts, R.; Lee, W.; Gautam, B. R.; Lee, S.; Lee, C.; Kim, T.; Kim, F. S.; Gundogdu, K.; Kim, B. J. Impact of highly crystalline, isoindigo-based small-molecular additives for

- enhancing the performance of all-polymer solar cells. *J. Mater. Chem.* A **2017**, *5*, 21291–21299.
- (66) Lee, C.; Kang, H.; Lee, W.; Kim, T.; Kim, K. H.; Woo, H. Y.; Wang, C.; Kim, B. J. High-performance all-polymer solar cells via sidechain engineering of the polymer acceptor: the importance of the polymer packing structure and the nanoscale blend morphology. *Adv. Mater.* **2015**, *27*, 2466–2471.
- (67) Kim, A.; Park, C. G.; Park, S. H.; Kim, H. J.; Choi, S.; Kim, Y. U.; Jeong, C. H.; Chae, W. S.; Cho, M. J.; Choi, D. H. Highly efficient and highly stable terpolymer-based all-polymer solar cells with broad complementary absorption and robust morphology. *J. Mater. Chem. A* **2018**, *6*, 10095–10103.
- (68) Shi, S.; Yuan, J.; Ding, G.; Ford, M.; Lu, K.; Shi, G.; Sun, J.; Ling, X.; Li, Y.; Ma, W. Improved All-Polymer Solar Cell Performance by Using Matched Polymer Acceptor. *Adv. Funct. Mater.* **2016**, 26, 5669–5678.
- (69) Oh, J.; Kranthiraja, K.; Lee, C.; Gunasekar, K.; Kim, S.; Ma, B.; Kim, B. J.; Jin, S. H. Side-Chain Fluorination: An Effective Approach to Achieving High-Performance All-Polymer Solar Cells with Efficiency Exceeding 7. *Adv. Mater.* **2016**, *28*, 10016–10023.
- (70) Earmme, T.; Hwang, Y. J.; Subramaniyan, S.; Jenekhe, S. A. All-polymer bulk heterojuction solar cells with 4.8% efficiency achieved by solution processing from a co-solvent. *Adv. Mater.* **2014**, *26*, 6080–6085.
- (71) Huo, L.; Liu, T.; Sun, X.; Cai, Y.; Heeger, A. J.; Sun, Y. Single-Junction Organic Solar Cells Based on a Novel Wide-Bandgap Polymer with Efficiency of 9.7%. *Adv. Mater.* **2015**, *27*, 2938–2944.
- (72) Li, Z.; Lin, J. D. A.; Phan, H.; Sharenko, A.; Proctor, C. M.; Zalar, P.; Chen, Z.; Facchetti, A.; Nguyen, T.-Q. Competitive Absorption and Inefficient Exciton Harvesting: Lessons Learned from Bulk Heterojunction Organic Photovoltaics Utilizing the Polymer Acceptor P(NDI2OD-T2). Adv. Funct. Mater. 2014, 24, 6989–6998.
- (73) Cowan, S. R.; Roy, A.; Heeger, A. J. Recombination in polymer-fullerene bulk heterojunction solar cells. *Phys. Rev. B: Condens. Matter Mater. Phys.* **2010**, 82, 245207.
- (74) Wetzelaer, G. A. H.; Kuik, M.; Lenes, M.; Blom, P. W. M. Origin of the dark-current ideality factor in polymer:fullerene bulk heterojunction solar cells. *Appl. Phys. Lett.* **2011**, *99*, 153506.
- (75) Kirchartz, T.; Deledalle, F.; Tuladhar, P. S.; Durrant, J. R.; Nelson, J. On the Differences between Dark and Light Ideality Factor in Polymer: Fullerene Solar Cells. *J. Phys. Chem. Lett.* **2013**, *4*, 2371–2376.
- (76) Ye, L.; Jiao, X.; Zhou, M.; Zhang, S.; Yao, H.; Zhao, W.; Xia, A.; Ade, H.; Hou, J. Manipulating Aggregation and Molecular Orientation in All-Polymer Photovoltaic Cells. *Adv. Mater.* **2015**, *27*, 6046–6054.
- (77) Müller-Buschbaum, P. The Active Layer Morphology of Organic Solar Cells Probed with Grazing Incidence Scattering Techniques. *Adv. Mater.* **2014**, *26*, 7692–7709.
- (78) Smilgies, D. M. Scherrer grain-size analysis adapted to grazing-incidence scattering with area detectors. *J. Appl. Crystallogr.* **2009**, 42, 1030–1034.